IET Microwaves, Antennas & Propagation

Research Article

Water-loaded metal diagonal horn applicator for hyperthermia

ISSN 1751-8725
Received on 12th August 2014
Accepted on 8th December 2014
doi: 10.1049/iet-map.2014.0699
www.ietdl.org

Soni Singh, Surya Pal Singh ✉

Department of Electronics Engineering, Indian Institute of Technology (BHU), Varanasi, UP 221 005, India
✉ *E-mail: spsingh.ece@iitbhu.ac.in*

Abstract: This study presents the design of water-loaded metal diagonal horn antenna at 2450 MHz along with simulation and experimental studies of specific absorption rate (SAR) and temperature distributions in a bio-medium (muscle) in direct contact with the water-loaded antenna for hyperthermia application. The metal diagonal horn is a multimode horn antenna, with identical aperture field distribution in the *E*- and *H*-planes. The SAR distribution in a phantom muscle in direct contact with water-loaded horn antenna measured at 2450 MHz is nearly in agreement with the corresponding simulated distribution. The simulation results for SAR distribution owing to diagonal horn are also compared with those owing to square aperture horn/box horn, of same aperture cross-section/broader dimension as the diagonal horn at 2450 MHz. The results indicate that the diagonal horn provides higher penetration depth/better transverse resolution over square aperture horn/box horn. In addition, the proposed diagonal horn provides circularly symmetric effective field size. Finally, thermal simulation results are also provided for the proposed applicator, which is in direct contact with a realistic model of muscle medium without and with small spherical as well as oval-shaped tumours of different dielectric properties embedded within the muscle medium.

1 Introduction

The focusing ability of microwave energy has aroused considerable research interest in its bio-medical applications for many years. Hyperthermia is one of the therapeutic modalities considered for cancer treatment. During hyperthermia treatment, the temperature of the tumour is raised in the range 43–50°C for a definite period resulting in the destruction of cancerous cells, while temperatures below 43°C is desired in tissue surrounding the tumour to avoid normal tissue damage. Heat therapy increases the efficacy of the chemotherapy and radiation therapy. Electromagnetic-induced hyperthermia is dependent upon specific absorption rate (SAR) (which is a function of microwave power, frequency, wave polarisation, dielectric properties and density of tumour), duration of treatment and blood flow rate. Radiofrequency (RF)/microwave power inputted to specific type of tumour through the applicator as well as duration of treatment should be optimised for the given frequency and polarisation of the wave to obtain adequate cytotoxicity. Further, heating is not instantaneous. Some time has to be spent before tumour temperature reaches the desired value (>43°C) [1]. Thermal optimisation can be performed to achieve one or more of the following goals: to achieve a target temperature distribution, to optimise heating of tumour compared to healthy tissue, avoidance of hot spots and maximised tumour coverage [2]. Various shapes of tumours that are observed in different regions of the body include spherical, oval and undulating [3]. Focusing of electromagnetic energy at the small spherical (or near spherical) tumour location is easily possible through symmetrical high-resolution exposure.

Many types of direct contact applicators are available in the literature for hyperthermia. These applicators include rectangular/square/circular/lucite cone waveguide applicators [4–7], multimodal applicator [8], dielectric lens/dielectric slab/dielectric loaded waveguide [9–13], conventional/modified box-horn antenna [14–16] and so on. The choice of applicator and hence microwave-induced hyperthermia depends on the factors already mentioned. By loading the applicator with high dielectric constant material, matching between the antenna and phantom bio-medium is improved, and also size of the antenna reduces considerably [12]. As leakage is minimum for direct contact applicators [17], these applicators are desirable as compared to spaced applicators.

Diagonal, conical, choke horns and annular cavity antennas may be grouped under the category of antennas providing symmetrical patterns [18–20]. However, significant difference of beamwidths is found in the principal planes of conical horn [19]. Choke horn and annular cavity antennas can provide perfect axis symmetrical beam, but they usually have low gain and provide wide beam [20]. However, diagonal horn has reasonable gain as well as beamwidth, and its radiation pattern in the far field possesses almost perfect circular symmetry so that the 3, 10 and 20 dB beamwidths are very closely equal, not only in the principal *E*- and *H*-planes, but also in the 45° and 135° planes [18]. Therefore the diagonal horn terminated in a phantom bio-medium may be one of the promising candidates for the treatment of localised spherical (or near spherical) tumours in superficial abdominal/thoracic/limb region of the body. Recently, two papers containing only the simulation study of TiO_2-loaded metal diagonal horn have been published in conference proceedings by our group [21, 22], but TiO_2 loading requires highly accurate machining of the ceramic material and hence is prone to experimental errors. To the best of the authors' knowledge, little work has been done till date in respect of the hyperthermia application of diagonal horn.

The objective of this paper is to investigate through simulation and experimentally the SAR and temperature distributions in a phantom muscle medium/realistic muscle model without or with spherical/oval tumours because of a promising direct contact water-loaded metal diagonal horn at 2450 MHz for hyperthermia application. All the numerical simulations have been carried out using Computer Simulation Technology Microwave Studio (CST MWS) 2011 software, which is based on finite integration numerical technique [23]. The experimental study of SAR distributions in the phantom bio-medium at 2450 MHz were carried out with the help of 50 Ω coaxial L-shaped and straight monopole probes and Agilent make spectrum analyser. The simulated results for SAR distribution in the phantom bio-medium at 2450 MHz are compared with the corresponding experimental results. The simulated values of penetration depth and effective field size (EFS) in the phantom bio-medium because of water-loaded metal diagonal horn at a frequency of 2450 MHz are also compared with

the respective parameter values owing to square aperture horn (carrying only TE_{10} mode) of same aperture cross-section as diagonal horn. Further, thermal simulations are performed for the proposed applicator designed at 2450 MHz, which is in direct contact with a realistic model of muscle medium without and with small spherical and oval-shaped tumours having different dielectric properties, embedded within the muscle medium.

2 Applicator design

Water-loaded metal diagonal horn was designed at the frequency of 2450 MHz following the procedure given by Love [18]. The horn designed at 2450 MHz was then fabricated using 0.2 cm thickness copper sheet. As shown in Fig. 1*a*, standard rectangular waveguide carrying TE_{10} mode is gradually transformed to circular waveguide carrying the TE_{11} mode. Another gradual transition converts the circular cross-sections into square, and the horn then flares out to the desired aperture size. All the cross-sections of the diagonal horn are square including the aperture. For small flare angles, the mode of propagation within the horn is principally such that the electric vector is parallel to one of the diagonals when the electric field is excited diagonally, and hence it is referred to as diagonal horn. Metal diagonal horn is a multimode horn antenna in which the internal field consists of superposition of the orthogonal TE_{10} and TE_{01} modes in the square waveguide. The design of metal diagonal horn is concerned with proper selection of the different dimensions of the horn to obtain minimum reflection coefficient at the operating frequency. Filling a waveguide by a dielectric with relative dielectric constant of ε_r, reduces the size of the antenna by a factor of $\sqrt{\varepsilon_r}$. The proposed horn is assumed to be filled with water. The complex permittivity of the water has been taken to be $77 - j12.09$ [15] at 2450 MHz. Higher frequency metal rectangular waveguide (WR-34) filled with water was used as input waveguide for operation at 2450 MHz.

Aperture dimension (d) of the water-loaded diagonal horn is selected for required gain (G), which can be found from the following relation [18]

$$G = 10 \log \frac{4\pi\eta d^2}{\lambda_w^2} \quad (1)$$

where η is the efficiency of the horn, which can be taken equal to 0.81 [18], and λ_w ($=\lambda/\sqrt{\varepsilon'_{rw}}$) is the effective wavelength at the design frequency of the horn, and ε'_{rw} is the real part of the relative permittivity of water. The proposed horn was designed for 15 dB gain. The aperture dimension 'd' found from (1) is given in Table 1. The proposed horn has a square aperture of dimension 'd' ($=1.7\lambda_w$) on each side corresponding to a flare angle of 18°. The throat dimension 'd_1' of the diagonal horn is selected in such a way that TE_{10} and TE_{01} modes propagate inside the square cross-section waveguide at the throat. Propagation of other higher-order modes is not allowed. To eliminate the higher-order modes, the throat dimension 'd_1' must be slightly greater than one-half wavelength, but less than three-half wavelengths [18]. The transformer lengths 'T_1' and 'T_2' of the rectangular-to-circular and circular-to-square waveguide transitions are selected on the basis of quarter wave transformer concept to obtain minimum reflection coefficient at the design frequency. The diameter 'D' of the circular waveguide is selected so that cut-off wavelength of rectangular waveguide carrying TE_{10} mode is equal to that of circular waveguide carrying TE_{11} mode. All the waveguide sections discussed earlier and the diagonal horn are assumed to be completely filled with water. The dimension optimisation of the proposed horn was carried out using CST MWS software.

The aperture of the diagonal horn is assumed to be surrounded by a conducting ground plane of copper in xy-plane so that the fringing electric field outside the aperture becomes zero. The dimensions of the conducting ground plane are $15 \times 15 \times 0.2$ cm^3 for the proposed horn. TE_{10} mode propagates in the input waveguide at the operating frequency of 2450 MHz. The input end of rectangular waveguide section of the horn is short circuited. The diagonal horn is assumed to be excited with the help of coaxial probe inserted through a small hole cut in the middle of the broad wall of rectangular waveguide section at a distance of $\lambda_{ge}/4$ from

Table 1 Design parameters of water-loaded metal diagonal horn

Parameter	Symbol	Dimension, mm
length of input waveguide	L_1	12
transition length of circular waveguide	T_1	10
length of circular waveguide	L_2	2
diameter of circular waveguide	D	10
transition length of square waveguide	T_2	13
length of square waveguide	L_3	4
throat size	d_1	9.1
length of flaring section	L	46
aperture size	d	24.6

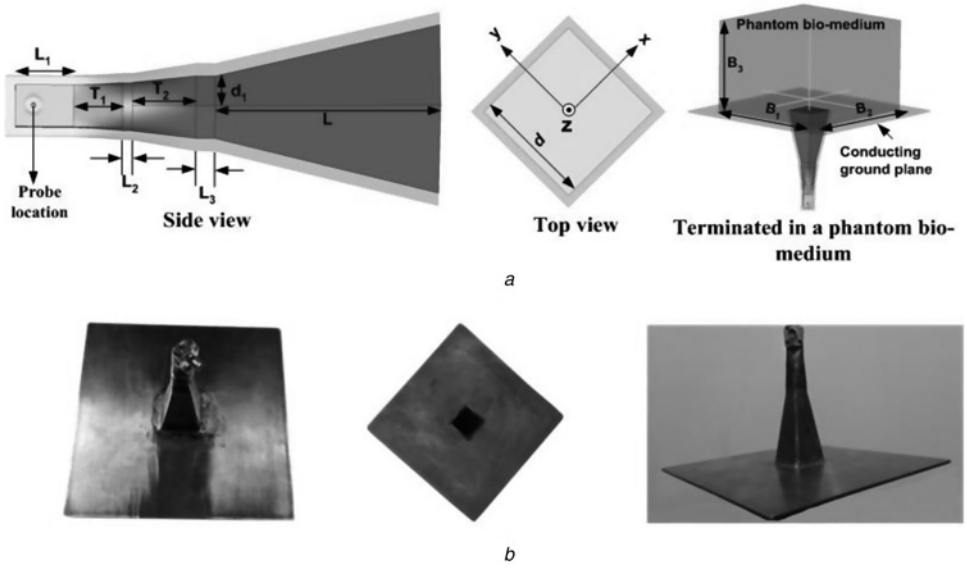

Fig. 1 *Metal diagonal horn design*

a Structure of metal diagonal horn antenna
b Different views of fabricated metal diagonal horn

the short circuited end, where $\lambda_{g\varepsilon}$ is the guide wavelength in water-loaded input rectangular waveguide for TE_{10} mode given by the relation

$$\lambda_{g\varepsilon} = \frac{\lambda_w}{\sqrt{1 - \left(f_{c_{10}}/f\right)^2}} \tag{2}$$

where λ_w ($= \lambda/\sqrt{\varepsilon'_{rw}}$) is already defined, $f_{c_{10}} = c/2a\sqrt{\varepsilon'_{rw}}$ is the cut-off frequency for TE_{10} mode, c is the velocity of microwave in free space $= 3 \times 10^8$ m/s, a is the broad dimension of the input rectangular waveguide and f is the operating frequency.

Fig. 1*b* shows different views of the fabricated horn for operation at 2450 MHz. SMA (Sub Miniature version A) connector was used for excitation of the water-loaded diagonal horn through coaxial probe at 2450 MHz.

3 Experimental technique for determination of SAR distributions inside the phantom bio-medium

For a given volume of the phantom bio-medium, SAR is proportional to the square of the magnitude of induced electric field strength inside the phantom bio-medium and is given by the relation

$$\text{SAR} = \frac{\sigma|E|^2}{2\rho} \tag{3}$$

where $|E|$ is the magnitude of total induced electric field strength inside the phantom bio-medium, and σ and ρ are the conductivity and density of the phantom bio-medium, respectively.

The experimental relative SAR distribution in the phantom bio-medium was determined at 2450 MHz with the help of Agilent make spectrum analyser (E4448A) and two 50 Ω coaxial monopole probes (one straight probe and another L-shaped probe). Equation (3) can be used to compute relative SAR value at the point in the phantom bio-medium if the power proportional to $|E|^2$ is measured for the given bio-medium. The laboratory grade distilled water was used to fill the diagonal horn shown in Fig. 1*b*. The material composition of the planar phantom bio-medium is taken to be 30% gelatin +69% water +1% NaCl [24]. The complex permittivity of the artificial phantom bio-medium (muscle medium) given in [24] is $50 - j16$ at 2450 MHz. The experimental setup for measuring the desired power level inside the phantom bio-medium in a particular direction owing to the proposed applicator is shown in Fig. 2*a*. The power proportional to square of the magnitude of *x*-/*y*-/*z*-component of induced electric field at a point inside the bio-medium owing to the applicator was detected with the help of coaxial monopole probes and spectrum analyser by keeping the axis of the corresponding probe along the particular *x*-/*y*-/*z*-direction (Fig. 2).

Agilent make analogue signal generator (E8257D) was connected to the fabricated water-loaded diagonal horn through Narda make step attenuator, HP (2–20 GHz, 20 dBm) microwave amplifier and Microlab make coaxial isolator as shown in Fig. 2*a*. A particular type of 50 Ω coaxial monopole probe was connected to the RF in port of the spectrum analyser through a flexible coaxial cable (procured from M/S. Vidyut Yantra Udyog, Modinagar, UP, India) as shown in Figs. 2*b* and *c*. The length and diameter of the extended inner conductor of straight coaxial probe are equal to 14 and 1.5 mm, respectively. The length and diameter of the extended inner conductor of L-shaped coaxial probe are equal to 12 and 1 mm, respectively. The power coupled from the analogue signal generator and power amplifier combination to the phantom bio-medium through the diagonal horn, which was designed and fabricated to operate at 2450 MHz, was sensed by a particular coaxial monopole probe. The spectrum analyser was configured to measure the power levels (in dBm) picked up by the probe, which was inserted inside the phantom bio-medium at 2450 MHz. The experimental determination of power level inside the phantom bio-medium which is proportional to square of the magnitude of *x*-/*y*-/*z*-component of induced electric field was carried out as detailed below. The power level corresponding to *z*- component of the induced field at a point in the phantom bio-medium which is proportional to $|E_z|^2$ was measured as a function of distance along *x*-/*y*-/*z*-direction by keeping the axis of the straight probe along the *z*-direction and moving it along the desired *x*-/*y*-/*z*-direction while keeping remaining coordinates fixed. The power levels corresponding to *x*- and *y*-components of the induced electric field at a point inside the phantom bio-medium which are proportional to the $|E_x|^2$ and $|E_y^2|$, respectively, were measured as a function of distance along *x*-/*y*-/*z*-direction by keeping the axis of the L-shaped probe along the *x*-/*y*-direction and moving it along the desired *x*-/*y*-/*z*-direction while keeping other coordinates fixed. The magnitude of the field component $|E_z|^2$ is small as compared to $|E_x|^2$ and $|E_y|^2$, however $|E_x|^2$ and $|E_y|^2$ are nearly same. The power proportional to square of the magnitude of each electric field component was sampled at a number of positions from 0 to ±11.2 cm along each of the *x*- and *y*-directions and from 0 to 8 cm along the *z*-direction for water-loaded diagonal horn operating at 2450 MHz. The differing responses of 50 Ω L-shaped and straight

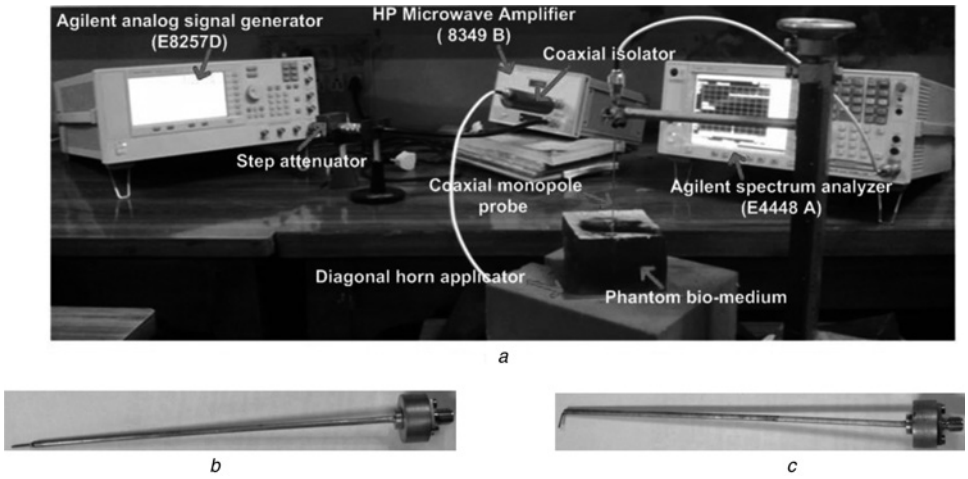

Fig. 2 *Experimental setup and coaxial monopole probe*

a Experimental setup for measurement of power level (proportional to square of the magnitude of induced electric field) in the phantom bio-medium
b Coaxial straight monopole probe
c Coaxial L-shaped monopole probe

IET Microw. Antennas Propag., 2015, Vol. 9, Iss. 8, pp. 814–821

coaxial probes in measuring the square of the magnitude of same field component were calibrated out through the application of correction factor.

The total induced electric field inside the phantom bio-medium at a particular point is given by

$$|E|^2 = |E_x|^2 + |E_y|^2 + |E_z|^2 \quad (4)$$

where E_x, E_y and E_z are the induced electric field components along x-, y- and z-directions, respectively.

The measured power levels at different points inside the phantom muscle medium were converted to experimental relative SAR distribution through the application of (3) and (4).

4 Results and discussion

The applicator's design data and dielectric property of phantom bio-medium (muscle medium) given in Sections 2 and 3 have been used to obtain the simulated value of input reflection coefficient of the water-loaded diagonal horn antenna in direct contact with the phantom bio-medium (muscle medium) at the operating frequency. The simulated and measured values of input reflection coefficient of the proposed antenna terminated in a phantom bio-medium are −17 and −12.9 dB, respectively, at 2450 MHz.

The density and conductivity of the phantom muscle medium used in simulation study of SAR distribution are equal to 1050 kg/m^3 and 2.1787 S/m [24], respectively. The simulated relative SAR distributions inside the phantom bio-medium (muscle) of size $B_1 \times B_2 \times B_3$ (=112 × 112 × 80 mm^3) at 2450 MHz owing to the proposed horn are determined using CST MWS software and the results are shown in Fig. 3. Initially, the power fed to the antenna was assumed to be 1 W in the simulation study. The relative SAR distributions in the phantom muscle medium are obtained by normalising the SAR values with respect to the maximum value of SAR that occurs in the phantom muscle medium.

For 1 W input power, the simulated value of peak SAR is 157 W/kg. However if the input power is increased to 2 and 3 W, the simulated values of peak SAR are enhanced to 314 and 471 W/kg, respectively. The simulated values of SAR at a depth of 1 cm for 1, 2 and 3 W input power are found to be 44.6, 89.2 and 133.7 W/kg, respectively.

The relative SAR distributions inside the phantom muscle measured with the help of coaxial monopole probes and spectrum analyser for the antenna operating at 2450 MHz are also shown in Fig. 3.

It can be seen from Fig. 3 that the measured and simulated SAR distributions are nearly in agreement with each other. It can also be observed from Fig. 3 that experimental values are deviating to a smaller degree from the corresponding simulated values. The deviation in the results may be due to the factors given below. The accuracy of the experimental results could be affected by the accuracy with which the position of the particular monopole probe is measured. For the present case accuracy of position measurement is ±0.2 cm. The finite size of the coaxial probe inserted inside the bio-medium may distort the induced electric field to some extent. Although these factors individually cannot cause much effect on the SAR value but when taken collectively, they may become significant cause of the deviation between the simulated and experimental relative SAR distributions.

Fig. 3*a* illustrates the relative SAR distribution in the homogeneous phantom muscle medium in the z-direction at 2450 MHz for the proposed horn. The values of simulated and experimental penetration depth in phantom bio-medium (depth where SAR value is down to 13.5% of the maximum in the muscle) extracted from Fig. 3*a* are given in Table 2 for diagonal

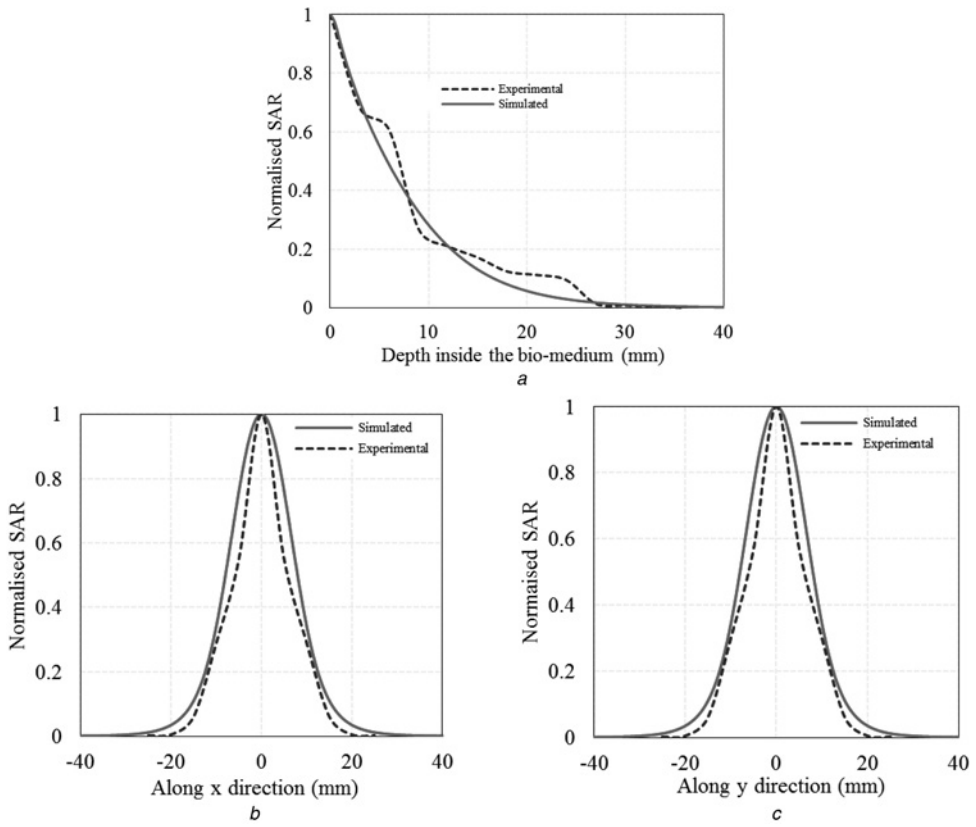

Fig. 3 *Relative SAR distributions inside the phantom bio-medium owing to proposed horn at 2450 MHz*

a Along the z-direction ($x = y = 0$)
b Along the x-direction at $z = 1$ cm ($y = 0$)
c Along the y-direction at $z = 1$ cm ($x = 0$)

Table 2 SAR parameters of water-loaded diagonal and square horns inside the phantom bio-medium at 2450 MHz

Type of applicator	Aperture size, cm^2	Gain, dB	EFS, cm^2		Penetration depth, cm	
			Simulated	Experimental	Simulated	Experimental
proposed antenna	2.46 × 2.46	15	1.6 × 1.6	1.3 × 1.3	1.5	1.7
square horn	2.46 × 2.46	15	1.35 × 2.1	–	1.3	–

Table 3 Thermal parameters of muscle for the BHE [26]

ρ, kg/m^3	C, kJ/kg °C	K, W/m °C	A_0, W/m^3	B, W/m^3 °C
1050	3.6	0.5	480	2700

horn designed at 2450 MHz. The values of simulated and experimental penetration depth are nearly in agreement with each other.

The EFS is defined as the area that is enclosed within 50% SAR contour inside the phantom bio-medium. Resolution of the applicator in transverse direction is represented by EFS and for high transverse resolution the value of EFS must be small. The simulated and experimental values of EFS extracted from Figs. 3*b* and *c* owing to the proposed horn are small, almost identical and exhibit circular symmetry (Table 2). Since diagonal horn is a multimode horn antenna which supports TE_{10} and TE_{01} modes, it shows identical aperture field distribution in *E*- and *H*-planes. That is why it exhibits circularly symmetric behaviour in the transverse plane.

4.1 Comparison of SAR distributions

The simulation results of SAR distribution inside the phantom bio-medium owing to proposed horn at 2450 MHz are compared with those because of square aperture horn (carrying only TE_{10} mode) of same aperture cross-section as diagonal horn. The simulated values of penetration depth and EFS inside the phantom bio-medium owing to square horn are listed in Table 2. The results indicate that diagonal horn provides slightly higher penetration depth as compared with square horn. The component of EFS in *E*-field direction in the bio-medium owing to square horn is much wider as compared to that in *H*-field direction, whereas EFS owing to diagonal horn exhibits circular symmetry.

The experimental values of penetration depth (=18 mm) and EFS (=39 × 38 mm^2) owing to conventional box horn of similar broader aperture size given in [15] are compared with those for the proposed horn at 2450 MHz. It can be observed from Table 2 and [15] that though the experimental penetration depth obtained owing to both applicators are comparable, but the experimental transverse resolution for the proposed horn is much better as compared with the applicator given in [15].

Hence, the proposed applicator can be a better choice for heating of small size spherical (or near spherical) tumours in superficial abdominal/thoracic/limb region of the body.

5 Simulation of temperature distribution in the realistic muscle model

The hyperthermia performance is characterised through the study of temperature distribution in the muscle. The heat generated by the electromagnetic energy absorbed in the muscle medium is proportional to SAR. The bio-heat equation represents the relationship between the rate of electromagnetic energy absorbed into the tissue and the resulting rise in tissue temperature. The temperature distribution inside the realistic muscle model can be evaluated by using Pennes' bio-heat equation (BHE) [25] given below

$$\rho C\frac{\partial T}{\partial t} = \nabla\cdot(K\nabla T) + A_0 + \rho\mathrm{SAR} - B(T - T_\mathrm{B}) \tag{5}$$

where ρ is the muscle density, C is the specific heat of muscle, K is the muscle thermal conductivity, A_0 is the metabolic heat production, B is heat exchange mechanism owing to capillary blood perfusion and T_B is the blood temperature assumed to be constant (=37°C, the normal body temperature).

In order to characterise the hyperthermia treatment system, muscle fed through water-loaded diagonal horn at 2450 MHz was considered as shown in Fig. 1*a*. The thermal simulation was performed by CST multi-physics simulator [23] software at an initial temperature of 37°C. The thermal parameters of the muscle used in simulation are listed in Table 3. Temperature distribution inside the muscle medium was simulated for three values of input power (=1, 2 and 3 W) fed to the proposed horn. Figs. 4*a* and *b* show the variations of temperature as functions of depth and time, respectively, at a point ($x = y = 0$, $z = 1$ cm) in the muscle medium by taking input power as a parameter. It can be seen from Fig. 4*a* that as the input power to the applicator increases, the peak value of temperature rises. As expected, the temperature decreases exponentially with depth inside the muscle medium. When the

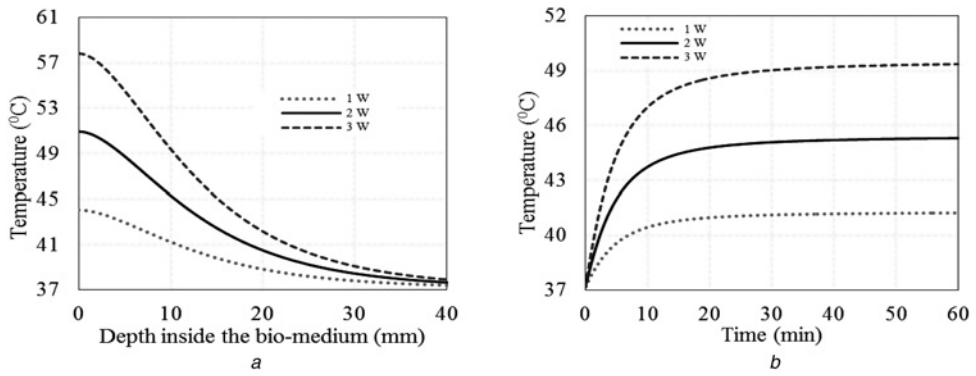

Fig. 4 *Temperature distribution inside the phantom muscle owing to proposed horn at 2450 MHz for different input power*

a Along the *z*-direction ($x = y = 0$)
b With respect to time at $z = 1$ cm ($x = y = 0$)

IET Microw. Antennas Propag., 2015, Vol. 9, Iss. 8, pp. 814–821

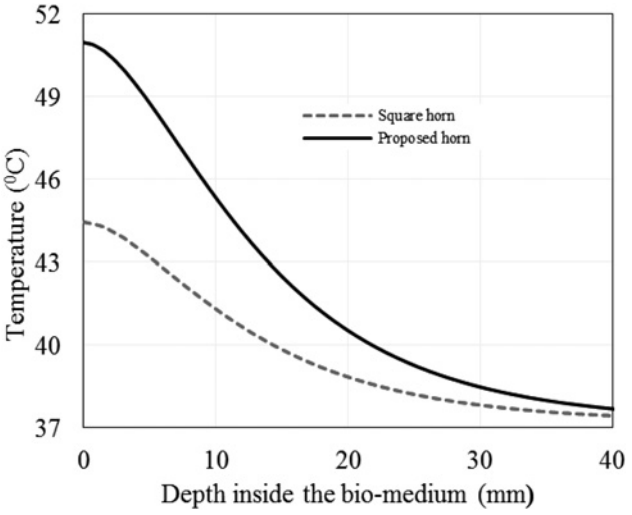

Fig. 5 *Temperature distribution inside the phantom muscle owing to proposed horn and square aperture horn at 2450 MHz for 2 W input power along the z-direction (x = y = 0)*

input power is 2 W, the muscle temperature at the point ($x = y = 0$, $z = 1$ cm) saturates at 45.3°C, which is well within the desired hyperthermia range (Fig. 4*b*). The temperature rise produced in living tissues by microwave heating is strongly a non-linear function of heating time. This fact is illustrated in Fig. 4*b*, in which initially rate of rise of temperature is higher for a given input power. The rate of rise of temperature slows down after 20 min of heating and the tissue temperature approaches a steady temperature after 30 min of heating for a given input power. However, the rate of change of temperature (dT/dt) at a given instant remains almost constant as input power increases. It is also observed that with 1 W input power the temperature at the point ($x = y = 0$, $z = 1$ cm) rises to a maximum of only 41.2°C, while with input powers of 2 and 3 W, temperature rises to maximum values of 45.3 and 49.36°C, respectively. The results demonstrate that for a given input power tissue temperature saturates after certain time period of heating and it rises in proportion to the input power at the given instant. It can be inferred from Fig. 4 that for effective hyperthermia treatment of superficial tumours, average duration of heating of 30–40 min after saturation at a temperature greater than 43°C using 2 W input power is optimum.

Further, the temperature distribution along the z-direction (for $x = y = 0$) in the tissue owing to proposed horn for 2 W input power is compared with that of the square horn of same aperture size carrying TE_{10} mode (Fig. 5). It can be observed from Fig. 5 that tissue temperature rises to a maximum of 50.9°C, whereas for square waveguide horn, the maximum temperature was only 44°C for the same input power. This is because the proposed horn is a multimode horn, in which there is more concentration of electric field in the central region of the aperture in comparison to square horn of same aperture size carrying only TE_{10} mode. Hence, it can be said that the proposed horn is more efficient hyperthermia applicator as compared to square horn.

The performance of the proposed applicator is now considered with a realistic muscle model consisting of a superficial spherical tumour (diameter = 16 mm)/oval-shaped tumour (semi-axes along the x-, y- and z-directions = 8, 8 and 7 mm) lying inside the muscle tissue as shown in Fig. 6*a*. The location of spherical/oval tumour is provided in Fig. 6*a*. The blood flow in spherical/oval tumour is assumed to be one-fourth of the value for the normal tissue [9]. It is well known that tumour has higher water content [27]. This

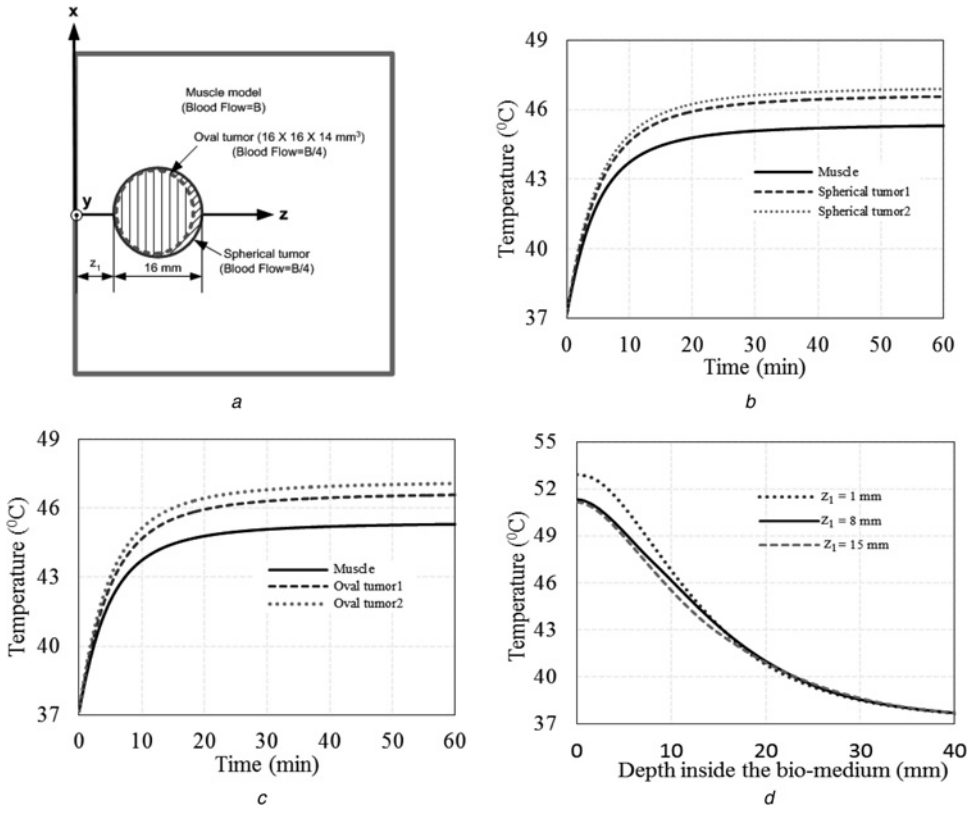

Fig. 6 *Two-dimensional realistic muscle model and temperature distribution inside the muscle medium owing to proposed horn at 2450 MHz for 2 W input power*

a Muscle model with spherical/oval tumour
b Temperature distribution with spherical tumour ($z_1 = 1$ mm) at ($x = y = 0$, $z = 1$ cm)
c Temperature distribution with oval tumour ($z_1 = 1$ mm) at ($x = y = 0$, $z = 1$ cm)
d Temperature distribution with spherical tumour1 along the depth

Table 4 Dielectric properties of tumour and muscle

Tissue type	ε'	σ, S/m	Temperature (°C) obtained at the point ($x = y = 0$, $z = 1$ cm)
muscle	50	2.1787	45.3
spherical tumour1	56	2.98	46.56
spherical tumour2	60	3.54	46.89
oval tumour1	56	2.98	46.58
oval tumour2	60	3.54	47.07

makes the dielectric constant and conductivity of tumour slightly higher as compared with normal muscle. To perceive the effect of variation in temperature distribution owing to different dielectric properties of tumour, two different values of dielectric properties of tumour (both spherical and oval shaped) are considered in the present study (Table 4).

If normal muscle tissue of Fig. 1*a* is replaced by the model of Fig. 6*a*, it can be observed from the variation of heating pattern as a function of time at the point ($x = y = 0$, $z = 1$ cm) that tumour (spherical/oval shaped) temperature reaches to higher values as compared with normal muscle temperature (Figs. 6*b* and *c* and Table 4). Further, it is observed that tumour temperature is increased with increase in its dielectric constant and conductivity. This would aid in effective preferential heating of superficial tumour in comparison to normal tissue. As can be seen from Fig. 6*d* that superficial spherical tumour is effectively heated using the proposed applicator, but its effectiveness in treating whole tumour volume is reduced when the tumour is seated at greater depth in the bio-medium. For heating of relatively large spherical (or nearly spherical) tumour at greater depth, an applicator at lower frequency (750 or 433 MHz) can be used.

Figs. 7 and 8 show the profiles of temperature distribution inside the realistic bio-medium without and with spherical tumour owing to the proposed applicator. It is observed that presence of tumour within the realistic muscle medium makes the peak temperature of the muscle medium rise. Owing to increase in conductivity and reduction in blood flow rate in the tumour region compared to the normal tissue, higher temperature rise is noticed in the tumour volume as compared to the normal muscle tissue. Symmetrical temperature distribution in the bio-medium owing to the proposed applicator can be observed in the transverse *xy*-plane (Figs. 7*c* and 8*c*). It can be seen from Fig. 8*c* that desired temperature range (43–50°C) for hyperthermia exists in the spherical tumour (Fig. 8).

From this study, one can infer that through proper thermal optimisation, focused heating of target (tumour) is possible.

6 Conclusion

Water-loaded metal diagonal horn has been investigated as hyperthermia applicator through simulation and experimentally at 2450 MHz. The study involved determination of simulated and experimental SAR distributions in the phantom muscle medium owing to the proposed horn. The SAR distribution owing to proposed horn has also been compared with those because of square aperture horn/box horn of same aperture cross-section/broader dimension at 2450 MHz. In addition, thermal simulations have also been performed on realistic muscle model without and with small spherical/oval tumour embedded inside the muscle medium owing to the proposed horn designed at 2450 MHz. The results of SAR distribution show that higher penetration depth in the phantom muscle owing to the proposed horn has been obtained as compared with square aperture horn. The simulated value of EFS owing to the proposed horn is approximately similar to those obtained using square aperture horn; however, the EFS owing to the proposed horn has circular symmetry. It has also been observed that the proposed horn provides much better transverse resolution compared to box horn. The thermal simulation results show that the heating pattern could be controlled by the input power, blood flow and dielectric properties of muscle medium. The temperature distribution in the single homogeneous muscle layer obtained through thermal simulation indicates that the

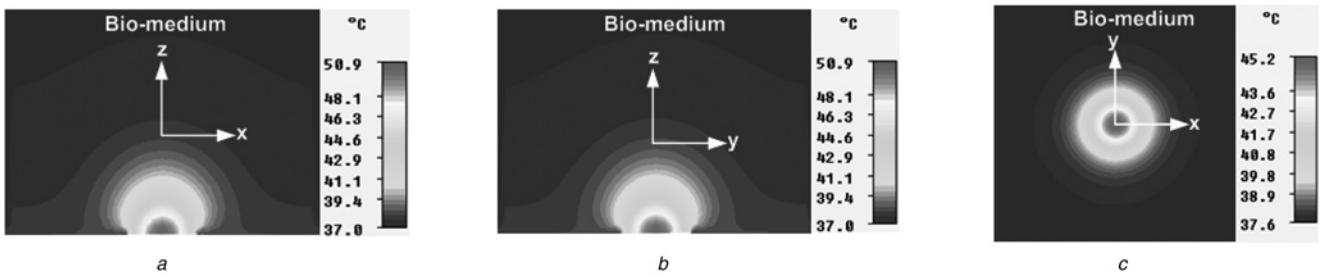

Fig. 7 *Temperature distribution inside the bio-medium at 2450 MHz owing to proposed horn*

a In the *xz*-plane ($y = 0$ cm)
b In the *yz*-plane ($x = 0$ cm)
c In the *xy*-plane at ($z = 1$ cm)

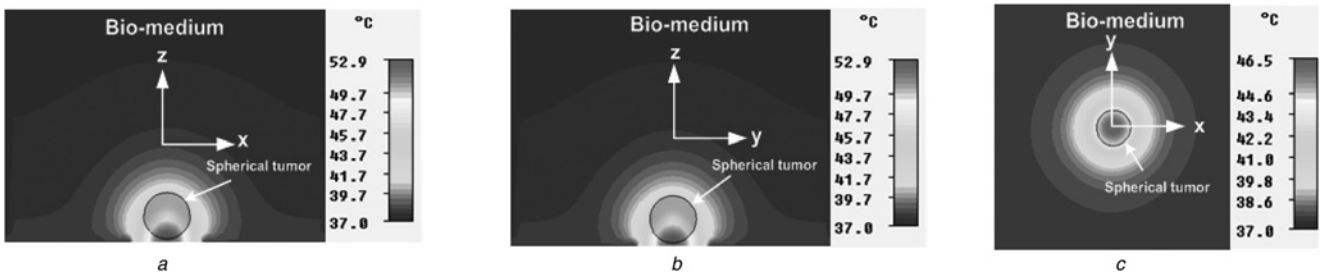

Fig. 8 *Temperature distribution inside the bio-medium embedded with spherical tumour ($z_1 = 1$ mm) at 2450 MHz owing to proposed horn*

a In the *xz*-plane ($y = 0$ cm)
b In the *yz*-plane ($x = 0$ cm)
c In the *xy*-plane at ($z = 1$ cm)

IET Microw. Antennas Propag., 2015, Vol. 9, Iss. 8, pp. 814–821

proposed horn can be used as effective hyperthermia applicator for spherical/near spherical tumours in superficial regions of the body by feeding relatively low power (2 W used in the present study), assuming that blood flow in the tumour region is reduced as compared with normal tissue region. For treating large undulating type of superficial tumours, the proposed applicator can be moved from one location to another after desired period of time. In case of real multilayer bio-media, because of impedance mismatch created owing to intervening fat layer in the abdominal/thoracic/limb region of the body, input power has to be increased to obtain desired temperature distribution in the muscle layer (the site of tumour) for effective hyperthermia.

7 References

1 Hahn, G.M.: 'Hyperthermia for the engineer: a short biological primer', *IEEE Trans. Biomed. Eng.*, 1984, **BME-31**, (1), pp. 3–8
2 Paulides, M.M., Stauffer, P.R., Neufeld, E., *et al.*: 'Simulation techniques in hyperthermia treatment planning', *Int. J. Hyperthermia (UK)*, 2013, **29**, (4), pp. 346–357
3 Agrawal, G., Su, M.-Y., Nalcioglu, O., Feig, S.A., Chen, J.-H.C.: 'Significance of breast lesion descriptors in the ACR BI-RADS MRI lexicon', *Cancer*, 2009, **115**, (7), pp. 1363–80
4 Guy, A.W., Lehmann, J.F., Stonebride, J.B., Sorenson, C.C.: 'Development of 915 MHz direct-contact applicator for therapeutic heating of tissues', *IEEE Trans. Microw. Theory Tech.*, 1978, **MTT-26**, (8), pp. 550–556
5 Lehmann, J.F., Guy, A.W., Stonebride, J.B., DeLateur, B.J.: 'Evaluation of a therapeutic direct contact 915 MHz microwave applicator for effective deep-tissue heating in humans', *IEEE Trans. Microw. Theory Tech.*, 1978, **MTT-26**, (8), pp. 556–563
6 Stuchly, M.A., Stuchly, S.S., Kantor, G.: 'Diathermy applicators with circular aperture and corrugated flange', *IEEE Trans. Microw. Theory Tech.*, 1980, **MTT-28**, (3), pp. 267–271
7 Van Rhoon, G.C., Rietveld, P.J., Van der Zee, J.: 'A 433 MHz lucite cone waveguide applicator for superficial hyperthermia', *Int. J. Hyperthermia (UK)*, 1998, **14**, (1), pp. 13–27
8 Lin, J.C., Kantor, G., Ghods, A.: 'A class of new microwave therapeutic applicators', *Radio Sci.*, 1982, **17**, pp. 119S–123S
9 Nikawa, Y., Watanabe, H., Kikuchi, M., Mori, S.: 'A direct-contact microwave lens applicator with a microcomputer-controlled heating system for local hyperthermia', *IEEE Trans. Microw. Theory Tech.*, 1986, **MTT-34**, (5), pp. 626–630
10 Kantor, G., Witters, D.M.: 'A 2450 MHz slab-loaded direct contact applicator with choke', *IEEE Trans. Microw. Theory Tech.*, 1980, **MTT-28**, (12), pp. 1418–1422
11 Nikawa, Y., Okada, F.: 'Dielectric-loaded lens applicator for microwave hyperthermia', *IEEE Trans. Microw. Theory Tech.*, 1991, **MTT-39**, (7), pp. 1173–1177
12 Uzunoglu, N.K., Angelikas, E.A., Cosmidis, P.A.: 'A 432 MHz local hyperthermia system using an indirectly cooled water-loaded waveguide applicator', *IEEE Trans. Microw. Theory Tech.*, 1987, **MTT-35**, (2), pp. 106–111
13 Nikita, K.S., Uzunoglu, N.K.: 'Analysis of the power coupling from a waveguide hyperthermia applicator into a three-layered tissue model', *IEEE Trans. Microw. Theory Tech.*, 1989, **37**, (7), pp. 1794–1800
14 Gupta, R.C., Singh, S.P.: 'Analysis of the SAR distributions in three layered bio-media in direct contact with a water-loaded modified box-horn applicator', *IEEE Trans. Microw. Theory Tech.*, 2005, **53**, (9), pp. 2665–2671
15 Gupta, R.C., Singh, S.P.: 'Development and analysis of a microwave direct contact water-loaded box-horn applicator for therapeutic heating of bio-medium', *Prog. Electromagn. Res.*, 2006, **62**, pp. 217–235
16 Ebrahimi-Ganjeh, M.A., Attari, A.R.: 'Study of water bolus effect on SAR penetration depth and effective field size for local hyperthermia', *Prog. Electromagn. Res. B*, 2008, **4**, pp. 273–283
17 Kantor, G., Witters, D.M., Greiser, J.W.: 'The performance of a new direct-contact applicator for microwave diathermy', *IEEE Trans. Microw. Theory Tech.*, 1978, **MTT-26**, (8), pp. 563–568
18 Love, A.W.: 'Electromagnetic horn antennas' (IEEE Press, 1976)
19 Balanis, C.A.: 'Modern antenna handbook' (John Wiley and Sons, 2008)
20 Boriskin, A.V., Zhadobov, M., Steshenko, S., *et al.*: 'Enhancing exposure efficiency and uniformity using a choke ring antenna: application to bioelectromagnetic studies at 60 GHz', *IEEE Trans. Microw. Theory Tech.*, 2013, **61**, (5), pp. 2005–2014
21 Singh, S., Katare, K.K., Singh, S.P.: 'SAR distribution in phantom bio-medium due to TiO_2 loaded diagonal horn'. Proc. Students Conf. on Engineering and System (SCES), Allahabad, India, April 2013, pp. 1–5
22 Singh, S., Katare, K.K., Patre, S.R., Singh, S.P.: 'Performance comparison of SAR distributions in phantom bio-medium due to TiO_2 loaded metal diagonal and square horn antennas'. Proc. Int. Microwave and RF Conf. (IMARC), New Delhi, India, Dec. 2013, pp. 1–4
23 Computer Simulation Technology (CST) [Online]. Available: http://www.cst.com
24 Stuchly, M.A., Stuchly, S.S.: 'Dielectric properties of biological substances – Tabulated', *J. Microw. Power*, 1980, **15**, pp. 19–26
25 Pennes, H.H.: 'Analysis of tissue and arterial blood temperatures in the resting human forearm', *J. Appl. Physiol*, 1998, **85**, pp. 5–34
26 Gong, Y., Wang, G.: 'Superficial tumor hyperthermia with flat left-handed metamaterial lens', *Prog. Electromagn. Res.*, 2009, **98**, pp. 389–405
27 Michaelson, S.M., Lin, J.C.: 'Biological effects and health implications of radiofrequency radiation' (Plenum Press, 1987)